



Original Research Article

Intensification of Catalytic Oxidative Desulfurization by MCM41 Supported Ionic Liquid-Ti-HPMo Composite Activating H₂O₂ System and Mechanism Insight



Parastoo Seyedmohammadi¹, Neda Kouhzadi¹, Alireza Taheri^{*1, 2}

¹ Department of Chemistry, Ilam Branch, Islamic Azad University, Ilam, Iran

² Arta Shimi Alborz Technical, Engineering, Educational and Research Institute, Tehran, Iran

ARTICLE INFO



ARTICLE HISTORY

Submitted: 2023-08-11

Revised: 2023-09-09

Accepted: 2023-11-08

Available online: 2023-11-09

Manuscript ID: PCBR-2308-1278

Checked for Plagiarism: Yes

Language Editor: Dr. Fatimah Ramezani

Editor who Approved

Publication: Dr. S. L.Sanati, Afsaneh

DOI: 10.48309/pcbr.2023.411107.1278

KEYWORDS

Heteropoly phosphomolybdic Acid
Oxidative desulfurization
Organosilane
BMIM
Gasoline

ABSTRACT

A facile one-pot synthesis method was developed to produce a new hybrid heterogeneous catalyst for catalytic oxidation removal of sulfur-containing compounds from petroleum samples. The presented catalyst is a Cd substituted heteropoly phosphomolybdic acid (HPMo) based on ionic liquid, which is stabilized on mesoporous silica. The physicochemical investigation of the catalyst was studied using FTIR, SEM, BET, XRD, and TEM. The results of XRD and FTIR proved that manganese was included in the catalyst structure, and the catalyst kept its Keggin type structure. The percentage of sulfur compounds removed after performing the catalyst activity in different conditions including temperature, catalyst amount, reaction time, and oxidant ratio was measured by GC-FID. Using the presented catalyst, it is possible to perform green desulfurization in a very short time with low cost and high removal efficiency. The performance of the synthesized catalyst in optimal conditions on 4 types of real fuels was evaluated.

Citation: Parastoo Seyedmohammadi, Neda Kouhzadi, Alireza Taheri. Intensification of Catalytic Oxidative Desulfurization by MCM41 Supported Ionic Liquid-Cd-HPMo Composite Activating H₂O₂ System and Mechanism Insight. Prog. Chem. Biochem. Res., 6(4) (2023) 327-340

<https://doi.org/10.48309/10.48309/pcbr.2023.411107.1278>

https://www.pcbiochemres.com/article_182709.html



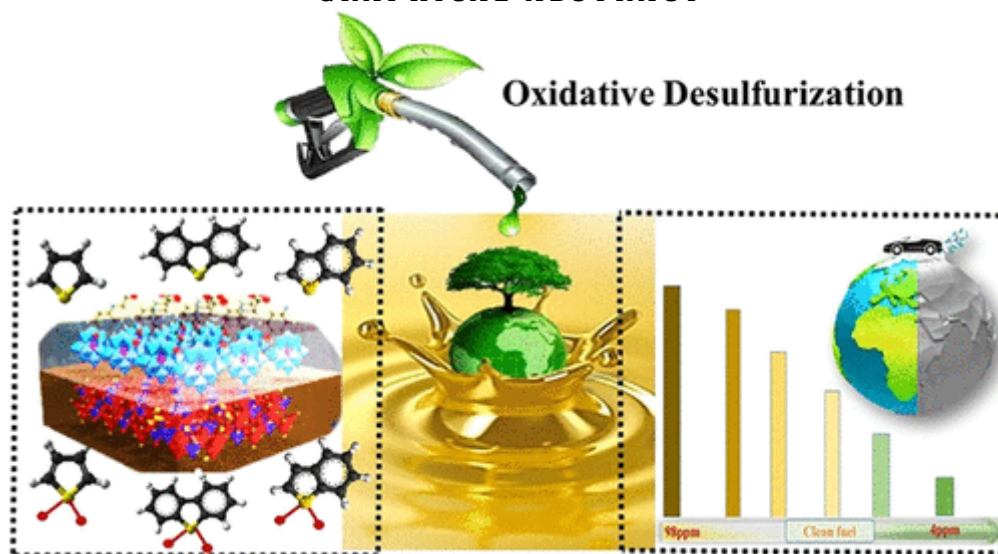
* Corresponding author: Alireza Taheri

✉ E-mail: alirezachem@yahoo.com

☎ Tel number: +9131061682

© 2023 by SPC (Sami Publishing Company)

GRAPHICAL ABSTRACT



1. INTRODUCTION

The ever-increasing growth of industries and the uncontrolled entry of chemicals into the environment, especially sulfur-containing chemicals, have caused serious environmental problems and adverse effects on human health [1,2]. Today, fossil fuels, which make up 82% of energy sources, are considered as the most important source of energy in the world [3]. Despite their useful applications in industrial, pharmaceutical, and medical fields, sulfur compounds in fossil fuels such as oil, gasoline, and diesel are considered as undesirable and polluting substances [4, 5]. In addition to soil and water, these pollutants are released in the surrounding air in the form of SO_x and NO_x gases [5]. To reduce the emission of suspended particles as well as sulfur oxides, international bodies imposed environmental restrictions and enacted laws. Hydro desulfurization (HDS) is the most common desulfurization method in refineries. In this process, some sulfur compounds such as thiophene, benzothiophene, and dibenzothiophene resist desulfurization due to alkylation [6]. Therefore, more temperature, pressure, time, and amount of catalyst will be required to reduce them. Accordingly, scientists have always sought to find methods with milder operating conditions and lower costs, such as oxidative, biological, absorption, and extraction desulfurization. Oxidative desulfurization process was first used in 1996 by Petrostar for

diesel desulfurization [6-9]. The catalytic-oxidative desulfurization process is one of the effective technologies with high efficiency to remove or reduce sulfur-containing compounds at low temperatures (less than 50 °C) and atmospheric pressure, which involves a chemical reaction between an oxidizing agent and sulfur-containing compounds [10-13]. In this process, compounds that have resisted the hydrogen desulfurization method are easily removed. Using this method, sulfur-containing organic compounds are converted into sulfones and sulfoxides by oxidizing agents, which can be easily separated from the non-polar phase of oil by processes such as extraction, absorption, and distillation. Oxidizing agent, type, amount of catalyst used, time, and temperature of oxidation are effective factors in oxidative desulfurization [14]. Organometallic frameworks can be used as effective heterogeneous catalysts in the oxidative desulfurization process due to their high surface area, functional groups, and design capability [15, 16]. Nanoporous materials are structures containing pores in the nano-size range, which recently provided conditions for the emergence of a new class of mesoporous structure called MCM41 [17-19]. This group of mesoporous compounds is easily produced and the materials used in their production are non-toxic, recyclable, and resistant to degradation caused by acidic compounds. In this research,

mesoporous zeolites are modified by organosilanes. They are a group of silicone compounds including alcohol and silica which are able to form bonds between organic compounds and minerals [20-23]. In this study, the structure and performance of the new heterogeneous nanocatalyst BMIM-Ti-HPMo MCM41, which was synthesized by the sol-gel method, is investigated.

2. EXPERIMENTAL

2.1. Materials and method

1-Butyl-3-methylimidazolium chloride (BMIM Cl), tetraethyl orthosilicate ($\text{SiC}_8\text{H}_{20}\text{O}_4$), and sodium molybdate dihydrate ($\text{Na}_2\text{MoO}_4 \cdot 2\text{H}_2\text{O}$) were obtained from Merck Company. DBT was obtained from Sigma-Aldrich Company. All the other chemicals used in this study were prepared with the analytical purity of Amertat-shimi Company (Tehran, Iran). In this research, a Binder GmbH- ED53 model electric oven was used to dry the samples. An electric furnace was purchased from Atbin Company for calcination, and YX2000A ultrasonic device was used to homogenize the samples. Gas chromatography-flame ionization detector (GC- FID) was used to measure the amount of analyte in the sample [24-26]. Prehydrotreated diesel fuel (density 0.7957 g mL^{-1} at 25°C and total sulfur content 481.80 mg/L) were sampled from Arak Petrochemical Company Co. Ltd. (Arak, Iran).

Catalytic-Oxidative desulfurization process of model fuel

In this research, the model fuel was obtained by dissolving the appropriate amount of dibenzothiophene in 50 ml of normal heptane and preparing a solution with a final concentration of 500 ppm. In each run, a certain amount of fuel was removed from the model. Then 50 mg of nanocatalyst and 3 ml of hydrogen peroxide were added to the reactor. The solution inside the reactor was stirred at a suitable temperature for a certain period of time. After the completion of the reaction, a certain volume of the oily phase was removed and sulfur-containing compounds in the fuel were determined using gas chromatography [26-30].

The removal percentage of sulfur-containing compounds is obtained from Equation (1):

$$x_i = (n_0 - n_i) / n_0 \times 100 \quad (1)$$

Where, x_i is the removal efficiency, n_0 is DBT concentration before the process, and n_i is the analyte concentration in the fuel after the process.

2.2.1. Synthesis the APTS/MCM41 nanocatalyst

About 1 g of calcined MCM41 and 5 mmol of aminopropyltrimethoxysilane (APTMS) were mixed in 30 g of anhydrous toluene and the mixture was refluxed for 12 h at 110°C [31]. The mixture was filtered and refluxed again with 15 ml of toluene for 24 h at 110°C , and then the obtained product (APTS/MCM41) was dried at 110°C for 24 h [32,33].

2.2.2. synthesis of BMIM-Ti-HPMo MCM41 nanocatalyst

APTS/MCM41 was dispersed in 50 ml, and then 9.1 mmol of disodium hydrogen phosphate (Na_2HPO_4), 100 mmol of dihydrate sodium molybdate ($\text{Na}_2\text{MoO}_4 \cdot 2\text{H}_2\text{O}$), and 12 mmol of Titanium nitrate ($\text{Ti}(\text{NO}_3)_2$) were added to it under vigorous stirring. Sodium hydroxide and hydrochloric acid were used to adjust pH at 4.8. Thereafter, 20 mmol of BMIM was slowly added to the solution at $80\text{--}85^\circ\text{C}$. The sediment was filtered and washed twice with a water-ethanol (1:1). Finally, recrystallization was done using acetonitrile. The nanocatalyst prepared in this step was called BMIM-Ti-HPMo-MCM41.

3. RESULT AND DISCUSSION

3.1. Characterizations of BMIM-Ti-HPMo- MCM41 nanocatalyst

Fig 1a displays FTIR of synthesized BMIM- Ti-HPMo MCM41 nanocatalyst. The peaks in the region of $800\text{--}1100 \text{ cm}^{-1}$ are assigned to the bending vibrations of regular and dense Si–O–Si network bonds. The peak in the region of 1048 cm^{-1} is assigned to the stretching vibrations of Si–OR bond. This indicates the formation of Si–O–Si bonds and confirms the formation of silicate structure [34, 35]. Due to the APTES addition in the second step, the absorption

spectra of 2851 and 2922 cm^{-1} can be assigned to the stretching vibrations of aliphatic carbons, and the peak of 1473 cm^{-1} is assigned to the bending vibrations of aliphatic carbons that indicates the APTES presence on the surface. The peak at 1644 cm^{-1} is assigned to the bending vibrations of NH_2 .

Fig 1b shows the X-ray diffraction pattern of the synthesized BMIM-Ti-HPMo-MCM41. The weak intensity of the peak at the angle of $2\theta = 1.181^\circ$ shows the lack of pore order in the MCM41 structure in the synthesized nanocatalyst. The peaks corresponding to the crystal planes of (100), (110), and (210) indicate the formation of a highly ordered hexagonal structure in the catalyst. The results indicate the presence of the pore in the MCM41 structure. In fact, the weakening of peaks in the sample is due to the filling of pores, which confirms the introduction of amine-containing functional groups into the mesopores [36, 37].

Using the scanning electron microscope in **Fig 1c and 1d**, the morphology of MCM41 and BMIM-Ti-HPMo MCM41 was investigated. In the SEM analysis of MCM41, the mesoporous channels and structures of MCM41 are clearly visible and these mesoporous structures are also visible in BMIM-Ti-HPMo-MCM41 with a slight change, which indicated the uniform distribution and formation of regular layers on the surface. The results of SEM analysis of BMIM-Ti-HPMo MCM41 and MCM41 consistent with the results of XRD and confirm the filling of internal pores and the formation of layers on the MCM41 surface in BMIM-Ti-HPMo-MCM41. In addition, a small number of fine agglomerations are also observed on the surface [38].

Fig 1e and 1f demonstrate the TEM analysis of MCM41 nanocatalyst base and synthesized BMIM-Ti-HPMo-MCM41 nanocatalyst. The TEM image related to the regular mesoporous structure of MCM41 clearly shows the uniform thickness of the wall in **Fig 1e** with black-white contrast. In **Fig 1f**, the 2-dimensional periodic meso-structures of the MCM41 were preserved even after the introduction of Mo and Ti into the pores, which is consistent with the XRD results. No agglomerations (big particles) were observed in the Figures, which indicates high dispersion and confinement of Mo and Ti species in the

channels of MCM41. This causes the pores to be filled and can be a reasonable explanation for the reduction in specific surface area [39].

The isothermal graph of nitrogen adsorption-desorption and the Barret Joyner-Halenda (BJH) of the MCM41 is type IV according to the IUPAC classification, which confirms the mesoporous nature of the porous composition (**Fig 2a and 2b**). The presence of a hysteresis cycle between the nitrogen absorption and desorption branch on the surface originates from the presence of capillary condensate in the mesoporous cavities, which is absorbed in the cylindrical cavities due to gas liquefaction. The delay during desorption is one of the characteristics of mesoporous materials (evaporation occurs at a lower relative pressure). As it is shown in isotherm graph, this hysteresis cycle can be seen in MCM41 between relative pressures of 0.55-0.75. The BET and BJH of the BMIM-Ti-HPMo-MCM41 shows the type IV isotherm [40].

The two graphs shown in **Fig 2a and 2b** are almost similar and staircase according to the reported reference, which is related to mesoporous materials. In this figure, the adsorption graph does not coincide with the desorption graph. According to the obtained results, the reduction of the specific surface area of MCM41 nanocatalyst base from 520.58 m^2/g to 150.89 m^2/g in BMIM-Ti-HPMo-MCM41 nanocatalyst indicates the addition of APTES and metal oxides into the pores, and as a result the pores are blocked and specific surface area and volume are decreased in the final synthesized nanocatalyst [41].

According to the size of the formed pores, the synthesized nanocatalyst can be classified in the mesoporous category. **Fig 2c** illustrates EDAX elemental analysis of BMIM-Ti-HPMo-MCM41 nanocatalyst. The spectra obtained from this analysis show the presence of elements such as Cd, O, Si, and Mo in the nanocatalyst. The weight percentages obtained from the elemental analysis of the nanocatalyst are consistent with the values considered for the nanocatalyst. In addition, the results of mapping images of Mo, Si, O, and Cd elements shown in **Figure 2d** confirm that Cd and Mo elements are uniformly distributed and dispersed in MCM41 channels. This shows that the surface of MCM41, which is a

silicate base, is covered in a large amount and in a multilayered manner. Based on the results of BET analysis, it can be concluded that the filling method is multilayered. These data are in acceptable agreement with the result of BET and XRD analyses.

3.2. Extractive-catalytic oxidative desulfurization (ECOD) experiments

A GC device (GC; Agilent, 7820A) with flame ionization detector and capillary column (Agilent

1909/z- 530.100m \times 250 μ m \times 0.5) was used for GC analysis. The results are shown in **Fig 3**. The analysis conditions of the GC are as follows: The carrier gas was nitrogen the temperature of the injector was 245 °C. The temperature of detector was 310°C. The temperature of the column was first 50 °C.

Then it was heated for 45 min with a temperature of 10 to 250°C. **Fig 3** shows DBT-STD and DBT- sulfone standards chromatographs and oxidation results after 30 and 65 °C.

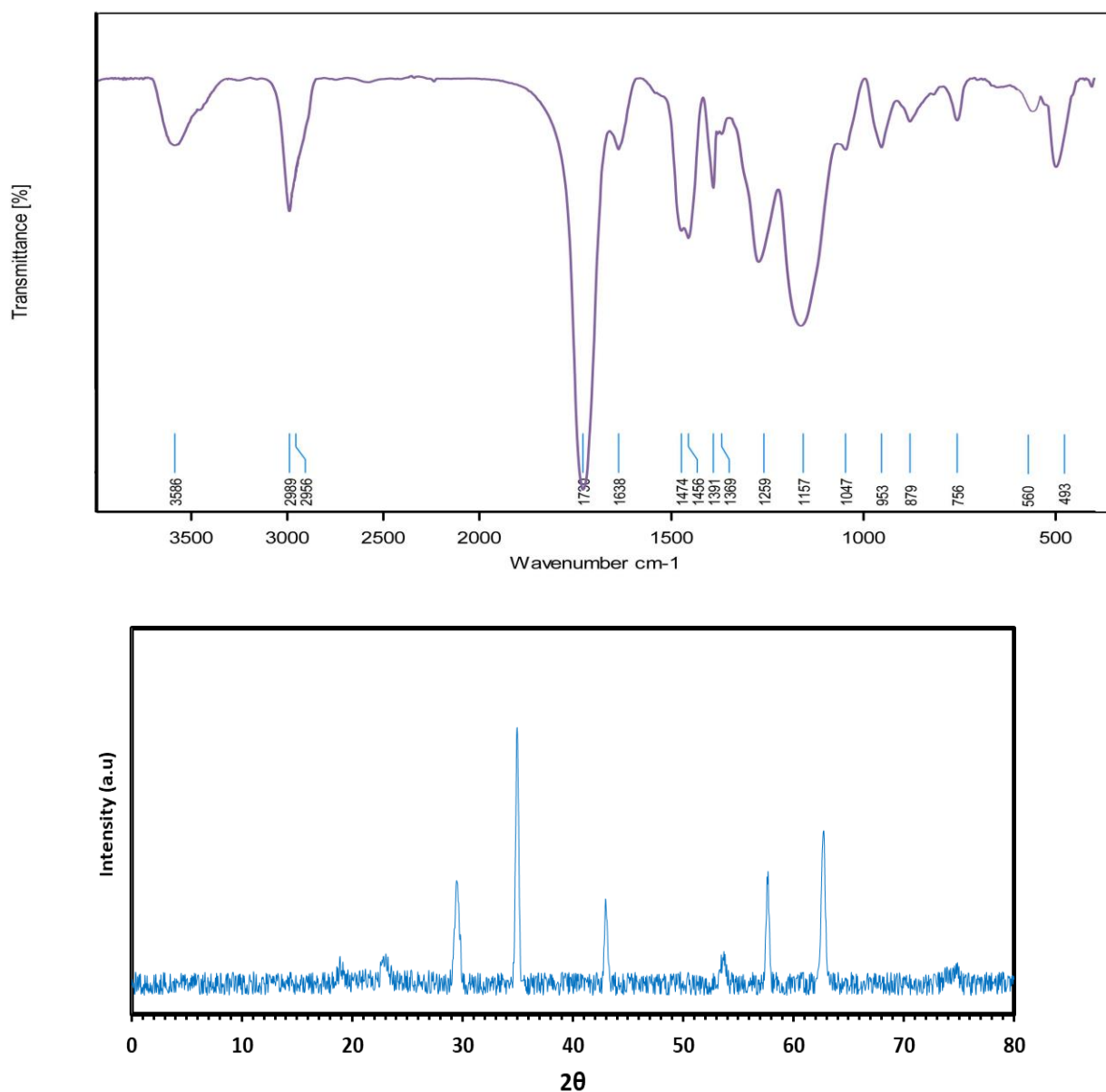


Fig 1.FTIR (a), XRD (b) of BMIM-Ti-HPMo MCM41, SEM of MCM41

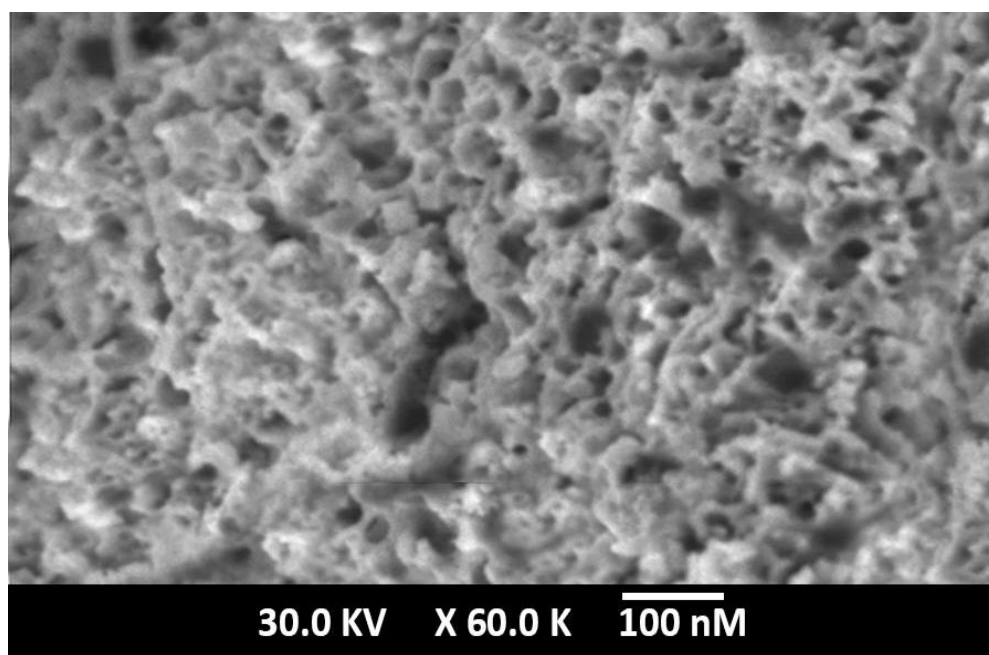
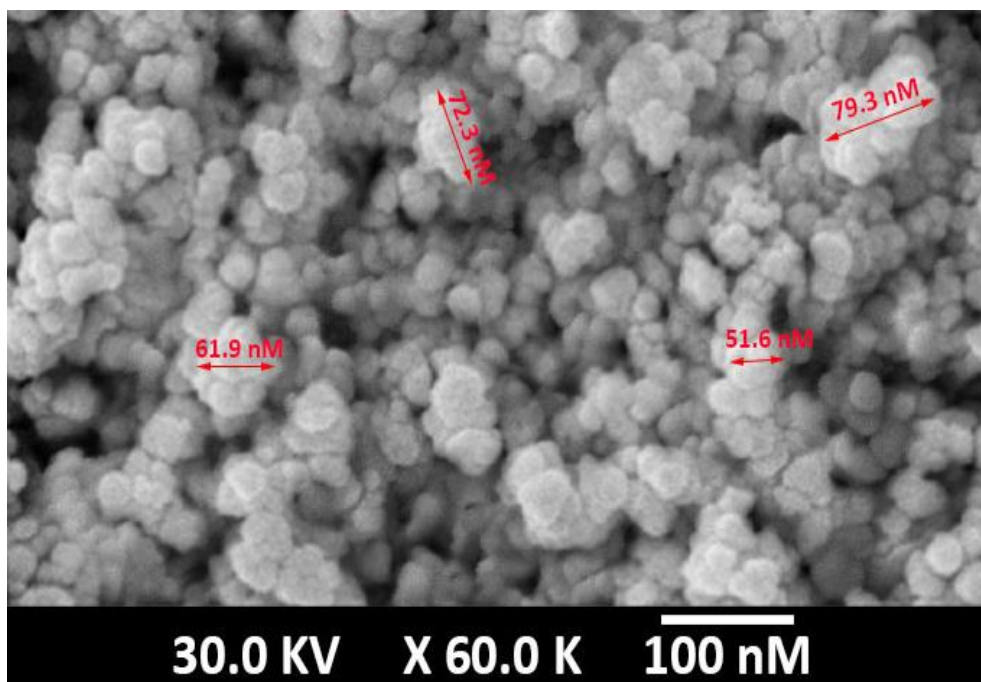


Fig 1 (continue) SEM of MCM41 (c) and BMIM-Ti-HPMo-MCM41

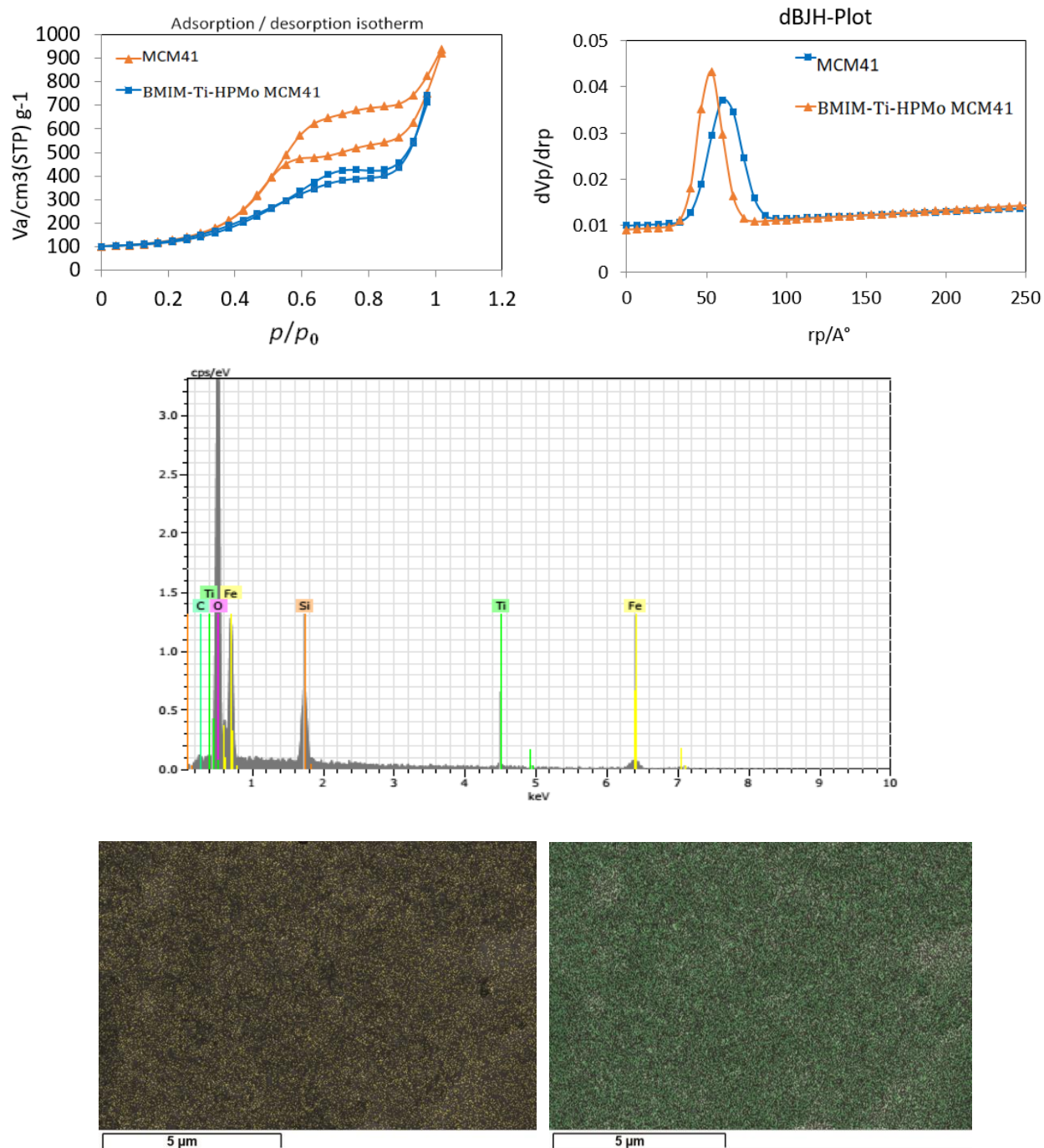


Fig 2. BET (a), EDAX analysis spectra (b), and mapping images (c) of BMIM-Ti-HPMo MCM41 nanocatalyst

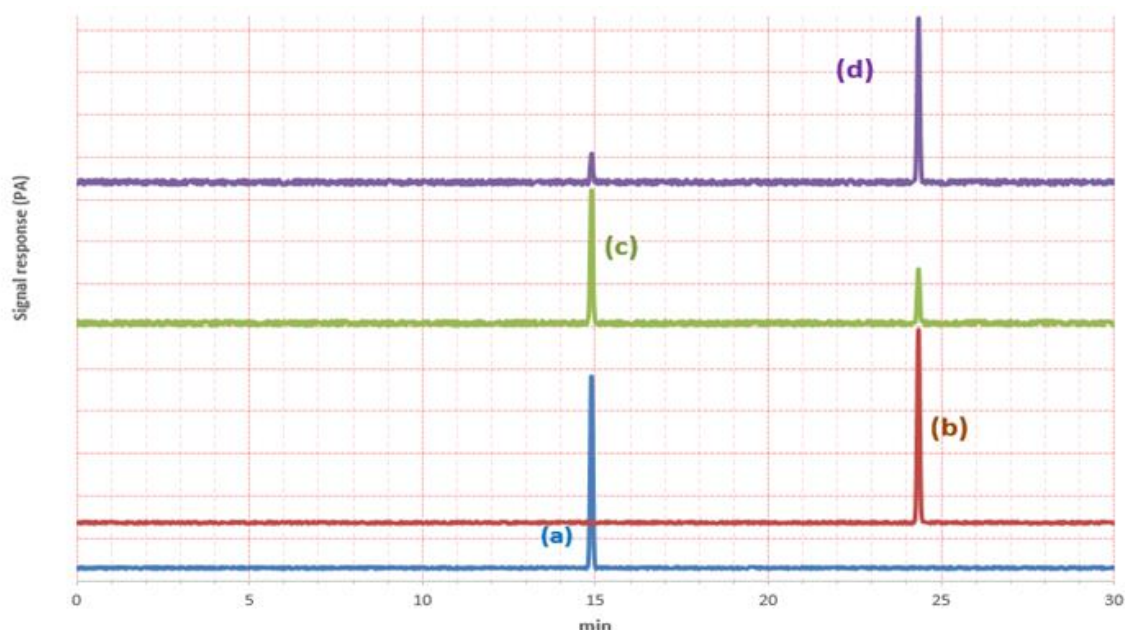


Fig 3.GC- FID chromatogram, DBT- STD (a) and DBT- sulfone – STD (b) diesel model fuel at 30 °C (c) and 65 °C (d)

3.2.1. Effect of temperature on the ECODS process

Temperature was evaluated as one of the effective parameters on the EODS process to remove sulfur- containing compounds of DBT. The effect of reaction temperature was investigated on the oxidative desulfurization process at temperatures of 40, 50, 60, and 70 °C. As it is shown in **Fig 4a**, the removal of DBT increases with increasing temperature from 40 to 60 °C. It can be concluded that increasing the temperature can increase the reaction rate and as a result the generation of active species is increased.

In addition, an increase in temperature leads to an increase in vapor pressure and catalytic activity and a decrease in liquid viscosity. Therefore, it leads to the reduction of the mass transfer limitation between the aqueous and organic phases. However, increasing the temperature to 70 °C does not have effect on the DBT removal.

3.2.2. Effect of oxidant ratio on the ECODS process

In the presence of BMIM-Ti-HPMo MCM41 nanocatalyst, the effect of the molar ratio of oxidant was investigated at 60 °C for 30 min contact time. The results are shown in **Fig 4b**. In this experiment, the ratios of 1:2, 1:1, 2:1, and 1:3 of hydrogen peroxide to acetic acid were used in the ECODS process. Hydrogen peroxide decomposes into hydroxyl radical to remove DBT. As it is shown in the figure, using a 1:3 ratio of hydrogen peroxide to acetic acid, the removal efficiency of DBT from the model fuel is increased.

3.2.3. Effect of catalyst dosage on the ECODS process

Fig 4c indicates the effect of the amount of BMIM-Ti-HPMo MCM41 nanocatalyst. By increasing the amount of nanocatalyst from 40 to 60 mg, the DBT removal efficiency increases. The cause of this behavior can be considered due to the increase of catalytic active sites. By increasing the amount of nanocatalyst to 70 mg, there is no significant change in the DBT removal.

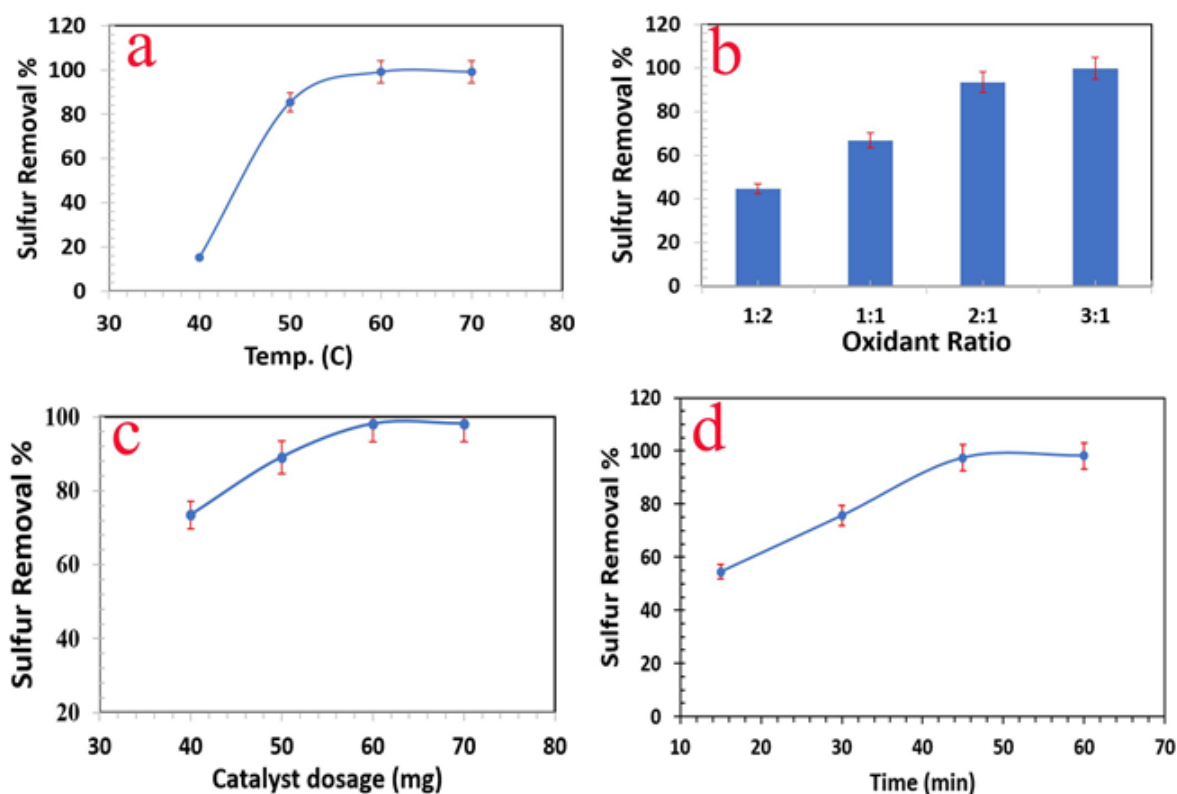


Fig 4. Effect of temperature (a), oxidant ratio (b), catalyst dosage (c) and reaction time (d)

Therefore, the optimal amount of BMIM-Ti-HPMo MCM41 nanocatalyst is 60 mg for DBT removal.

3.2.4. Effect of reaction time on the ECODS process

Fig 4d shows the effect of reaction time as an effective parameter on DBT removal in ECODS process. The highest amount of DBT removal was 98%, which took place in 45 min. Increasing the contact time did not have a significant effect on the removal of dibenzothiophene. At the initial times of the reaction, the catalytic active sites for oxidation are large, that's why a high percentage of dibenzothiophene is absorbed in 45 min. However, as the contact time increases, the adsorption sites are occupied and therefore, the amount of DBT adsorption by the nanocatalyst is gradually decreases.

3.2.5 Extractive-oxidative desulfurization of diesel fuel

Investigating the performance of heterogeneous hybrid nanocatalyst on the desulfurization of four diesel fuel sampled from Arak Petrochemical (Arak, Iran) was studied.

Fig 5 shows the results of DBT removal. As shown in the figure, the nanocatalyst has the ability to remove 98% of the residual sulfur content in diesel and gasoline. In this study, the removal efficiency of sulfur-containing compounds was studied at different times. From the mentioned figure, it can be deduced that the maximum amount of sulfur removal is done in the initial times (initial 20 min) and it takes 45 min for the removal to reach its maximum efficiency.

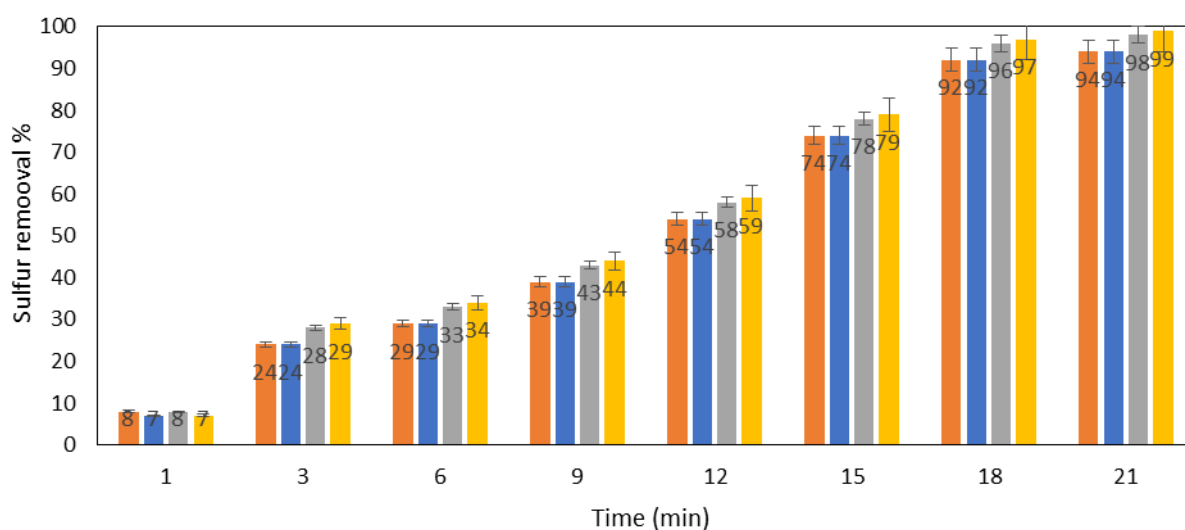


Fig 5. Sulfur removal of DBT from 4 Diesel fuel samples

4. Conclusion

In this study, a cetyltrimethylammonium bromide-manganese phosphomolybdate nanocatalyst stabilized on MCM41 modified with organosilane was synthesized. The structure of the heterogeneous hybrid nanocatalyst was investigated and catalytic-oxidative desulfurization of DBT in gasoline was studied. In addition, the effect of various operating parameters such as temperature, reaction time, oxidant ratios, and the amount of nanocatalyst was evaluated. In the structure of the nanocatalyst, ionic liquid (BMIM) has been used as a transfer agent. Manganese is introduced into the structure of the catalyst, and finally the nanocatalyst is immobilized on mesoporous zeolite MCM41. Optimum conditions for removing 98% of DBT from diesel fuel, including application of temperature of 60 °C for 45 min using 40 mg of nanocatalyst and oxidant ratio of 1:3, were obtained.

Funding

The authors declare that no funds, grants, or other support were received during the preparation of this manuscript.

Data availability

The datasets used and/or analyzed during the current study are available from the corresponding author on reasonable request.

Ethical approval

Not applicable.

Consent to participate

Not applicable.

Consent for publication

Not applicable.

CRedit authorship contribution statement

Neda Koohzadi: Data curation, writing original draft, preparation, and software.

Zahra Moafi: Methodology, visualization, investigation, software, and validation.

Alireza Taheri: Conceptualization, supervision, writing- reviewing and editing.

Declaration of Competing Interest

The authors declare that they have no known competing financial interests or personal relationships that could have appeared to influence the work reported in this paper

Acknowledgements

The authors are thankful to the Arta Shimi Alborz Technical, Engineering, Educational, and Research Institute, for providing research facilities.

ORCID

Alireza Taheri

<https://orcid.org/000-0003-3113-2148>

References

1. Lu X, Fan C, He W, Deng J, Yin H. Sulfur-containing amino acid methionine as the precursor of volatile organic sulfur compounds in algae-induced black bloom, *Journal of environmental sciences*; 2013 Jan 1; 25(1):33-43. [Crossref], [Google Scholar], [Publisher]
2. Mukwevho E, Ferreira Z, Ayeleso A. Potential role of sulfur-containing antioxidant systems in highly oxidative environments, *Molecules*; 2014 Nov 25; 19(12):19376-89. [Crossref], [Google Scholar], [Publisher]
3. Lin B, Ouyang X. A revisit of fossil-fuel subsidies in China: challenges and opportunities for energy price reform, *Energy Conversion and Management*; 2014 Jun 1; 82:124-34. [Crossref], [Google Scholar], [Publisher]
4. Soleimani M, Bassi A, Margaritis A. Biodesulfurization of refractory organic sulfur compounds in fossil fuels, *Biotechnology advances*; 2007 Nov 1; 25(6):570-96. [Crossref], [Google Scholar], [Publisher]
5. Mei H, Mei BW, Yen TF. A new method for obtaining ultra-low sulfur diesel fuel via ultrasound assisted oxidative desulfurization☆, *Fuel*; 2003 Mar 1; 82(4):405-14. [Crossref], [Google Scholar], [Publisher]
6. Choi KH, Korai Y, Mochida I, Ryu JW, Min W. Impact of removal extent of nitrogen species in gas oil on its HDS performance: an efficient approach to its ultra deep desulfurization, *Applied Catalysis B: Environmental*; 2004 Jun 18; 50(1):9-16. [Crossref], [Google Scholar], [Publisher]
7. Amoatey P, Omidvarborna H, Baawain MS, Al-Mamun A. Emissions and exposure assessments of SOX, NOX, PM10/2.5 and trace metals from oil industries: A review study (2000–2018), *Process Safety and Environmental Protection*; 2019 Mar 1; 123:215-28. [Crossref], [Google Scholar], [Publisher]
8. Eßer J, Wasserscheid P, Jess A. Deep desulfurization of oil refinery streams by extraction with ionic liquids, *Green chemistry*; 2004; 6(7):316-22. [Crossref], [Google Scholar], [Publisher]
9. Egorova M, Prins R. Hydrodesulfurization of dibenzothiophene and 4, 6-dimethyldibenzothiophene over sulfided NiMo/γ-Al₂O₃, CoMo/γ-Al₂O₃, and Mo/γ-Al₂O₃ catalysts, *Journal of Catalysis*; 2004 Jul 25; 225(2):417-27. [Crossref], [Google Scholar], [Publisher]
10. Ribeiro S, Barbosa AD, Gomes AC, Pillinger M, Gonçalves IS, Cunha-Silva L, Balula SS. Catalytic oxidative desulfurization systems based on Keggin phosphotungstate and metal-organic framework MIL-101, *Fuel processing technology*; 2013 Dec 1; 116:350-7. [Crossref], [Google Scholar], [Publisher]
11. Wu P, Liu P, Chen L, Ma W, Zhu L, Liu M, He J, Lu L, Chao Y, Zhu W. Synergistic effect of Au–Cu alloy nanoparticles on TiO₂ for efficient aerobic catalytic oxidative desulfurization, *Industrial & Engineering Chemistry Research*; 2022 Apr 28; 61(19):6292-300. [Crossref], [Google Scholar], [Publisher]
12. Xun S, Zhu W, Zheng D, Li H, Jiang W, Zhang M, Qin Y, Zhao Z, Li H. Supported ionic liquid [Bmim] FeCl₄/Am TiO₂ as an efficient catalyst


- for the catalytic oxidative desulfurization of fuels, *Rsc Advances*; 2015; 5(54):43528-36. [[Crossref](#)], [[Google Scholar](#)], [[Publisher](#)]
13. Lü H, Li P, Deng C, Ren W, Wang S, Liu P, Zhang H. Deep catalytic oxidative desulfurization (ODS) of dibenzothiophene (DBT) with oxalate-based deep eutectic solvents (DESs), *Chemical Communications*; 2015; 51(53):10703-6. [[Crossref](#)], [[Google Scholar](#)], [[Publisher](#)]
14. Eseva EA, Akopyan AV, Anisimov AV, Maksimov AL. Oxidative desulfurization of hydrocarbon feedstock using oxygen as oxidizing agent (a review), *Petroleum Chemistry*; 2020 Sep; 60:979-90. [[Crossref](#)], [[Google Scholar](#)], [[Publisher](#)]
15. Jose N, Sengupta S, Basu JK. Optimization of oxidative desulfurization of thiophene using Cu/titanium silicate-1 by box-behnken design, *Fuel*; 2011 Feb 1; 90(2):626-32. [[Crossref](#)], [[Google Scholar](#)], [[Publisher](#)]
16. Nawaf AT, Jarullah AT, Gheni SA, Mujtaba IM. Development of kinetic and process models for the oxidative desulfurization of light fuel, using experiments and the parameter estimation technique, *Industrial & Engineering Chemistry Research*; 2015 Dec 23; 54(50):12503-15. [[Crossref](#)], [[Google Scholar](#)], [[Publisher](#)]
17. Nguyen TT, Qian EW. Synthesis of mesoporous Ti-inserted MCM41 and CoMo/Ti-MCM41 catalyst for hydrodesulfurization and hydrodearomatization, *Microporous and Mesoporous Materials*; 2018 Jul 15; 265:1-7. [[Crossref](#)], [[Google Scholar](#)], [[Publisher](#)]
- [18] Liu YM, Cao Y, Yi N, Feng WL, Dai WL, Yan SR, He HY, Fan KN. Vanadium oxide supported on mesoporous MCM41 as highly selective catalysts in the oxidative dehydrogenation of propane, *Journal of Catalysis*; 2004 Jun 10; 224(2):417-28. [[Crossref](#)], [[Google Scholar](#)], [[Publisher](#)]
- [19] Babaei A, Aminikhah M, Taheri AR. A multi-walled carbon nano-tube and nickel hydroxide nano-particle composite-modified glassy carbon electrode as a new sensor for the sensitive simultaneous determination of ascorbic acid, dopamine and uric acid, *Sensor letters*; 2013 Feb 1; 11(2):413-22. [[Crossref](#)], [[Google Scholar](#)], [[Publisher](#)]
20. Alkan M, Tekin G, Namli H. FTIR and zeta potential measurements of sepiolite treated with some organosilanes, *Microporous and Mesoporous Materials*; 2005 Sep 15; 84(1-3):75-83. [[Crossref](#)], [[Google Scholar](#)], [[Publisher](#)]
21. Bonaccorsi L, Bruzzaniti P, Calabrese L, Proverbio E. Organosilanes functionalization of alumino-silica zeolites for water adsorption applications, *Microporous and Mesoporous Materials*; 2016 Nov 1; 234:113-9. [[Crossref](#)], [[Google Scholar](#)], [[Publisher](#)]
22. Borodina E, Karpov SI, Selemenev VF, Schwieger W, Maracke S, Fröba M, Rößner F. Surface and texture properties of mesoporous silica materials modified by silicon-organic compounds containing quaternary amino groups for their application in base-catalyzed reactions, *Microporous and Mesoporous Materials*; 2015 Feb 1; 203:224-31. [[Crossref](#)], [[Google Scholar](#)], [[Publisher](#)]
23. Faramarzi R, Taheri AR, Roushani M. Determination of paraquat in fruits and natural water using Ni (OH)₂ nanoparticles-carbon nanotubes composite modified carbon ionic liquid electrode, *Analytical & Bioanalytical Electrochemistry*; 2015 Dec 1; 7(6):666-83. [[Google Scholar](#)]
24. Sarafray-Yazdi A, Amiri AH, Es'Haghi Z. Separation and determination of benzene, toluene, ethylbenzene and o-xylene compounds in water using directly suspended droplet microextraction coupled with gas chromatography-flame ionization detector, *Talanta*; 2009 May 15; 78(3):936-41. [[Crossref](#)], [[Google Scholar](#)], [[Publisher](#)]
25. Yazdi AS, Razavi N, Yazdinejad SR. Separation and determination of amitriptyline and nortriptyline by dispersive liquid-liquid microextraction combined with gas chromatography flame ionization detection,

- Talanta*; 2008 Jun 15; 75(5):1293-9. [[Crossref](#)], [[Google Scholar](#)], [[Publisher](#)]
26. Farajzadeh MA, Mogaddam MR. Air-assisted liquid-liquid microextraction method as a novel microextraction technique; Application in extraction and preconcentration of phthalate esters in aqueous sample followed by gas chromatography-flame ionization detection, *Analytica chimica acta*; 2012 May 30; 728:31-8. [[Crossref](#)], [[Google Scholar](#)], [[Publisher](#)]
27. Haruna A, Merican ZM, Musa SG. Recent advances in catalytic oxidative desulfurization of fuel oil-A review, *Journal of Industrial and Engineering Chemistry*; 2022 Aug 25; 112:20-36. [[Crossref](#)], [[Google Scholar](#)], [[Publisher](#)]
28. Chica A, Corma A, Dómine ME. Catalytic oxidative desulfurization (ODS) of diesel fuel on a continuous fixed-bed reactor, *Journal of Catalysis*; 2006 Sep 10; 242(2):299-308. [[Crossref](#)], [[Google Scholar](#)], [[Publisher](#)]
29. Jiang W, Zhu W, Chang Y, Chao Y, Yin S, Liu H, Zhu F, Li H. Ionic liquid extraction and catalytic oxidative desulfurization of fuels using dialkylpiperidinium tetrachloroferrates catalysts, *Chemical Engineering Journal*; 2014 Aug 15; 250:48-54. [[Crossref](#)], [[Google Scholar](#)], [[Publisher](#)]
30. Abdollahi F, Taheri A, Shahmari M. Application of selective solid-phase extraction using a new core-shell-shell magnetic ion-imprinted polymer for the analysis of ultra-trace mercury in serum of gallstone patients, *Separation Science and Technology*; 2020 Oct 12; 55(15):2758-71. [[Crossref](#)], [[Google Scholar](#)], [[Publisher](#)]
31. Aghamohammadi S, Haghighi M, Maleki M, Rahemi N. Sequential impregnation vs. sol-gel synthesized Ni/Al₂O₃-CeO₂ nanocatalyst for dry reforming of methane: Effect of synthesis method and support promotion, *Molecular Catalysis*; 2017 Apr 1; 431:39-48. [[Crossref](#)], [[Google Scholar](#)], [[Publisher](#)]
32. Tao Q, Xu Z, Wang J, Liu F, Wan H, Zheng S. Adsorption of humic acid to aminopropyl functionalized MCM41, *Microporous and Mesoporous Materials*; 2010 Jun 1; 131(1-3):177-85. [[Crossref](#)], [[Google Scholar](#)], [[Publisher](#)]
33. Tu CH, Wang AQ, Zheng MY, Wang XD, Zhang T. Factors influencing the catalytic activity of MCM41-supported copper nanoparticles in CO oxidation, *Applied Catalysis A: General*; 2006 Jan 4; 297(1):40-7. [[Crossref](#)], [[Google Scholar](#)], [[Publisher](#)]
34. Luan Z, Fournier JA. In situ FTIR spectroscopic investigation of active sites and adsorbate interactions in mesoporous aluminosilicate MCM41 molecular sieves, *Microporous and Mesoporous Materials*; 2005 Apr 1; 79(1-3):235-40. [[Crossref](#)], [[Google Scholar](#)], [[Publisher](#)]
35. Mureseanu M, Reiss A, Stefanescu I, David E, Parvulescu V, Renard G, Hulea V. Modified MCM41 mesoporous silica for heavy metal ions remediation, *Chemosphere*; 2008 Nov 1; 73(9):1499-504. [[Crossref](#)], [[Google Scholar](#)], [[Publisher](#)]
36. Yan W, Petkov V, Mahurin SM, Overbury SH, Dai S. Powder XRD analysis and catalysis characterization of ultra-small gold nanoparticles deposited on titania-modified MCM41, *Catalysis Communications*; 2005 Jun 1; 6(6):404-8. [[Crossref](#)], [[Google Scholar](#)], [[Publisher](#)]
37. Zholobenko VL, Khodakov AY, Durand D. Synchrotron X-ray diffraction-diffusion studies of the preparation of MCM41 materials, *Microporous and mesoporous materials*; 2003 Dec 5; 66(2-3):297-302. [[Crossref](#)], [[Google Scholar](#)], [[Publisher](#)]
38. Wang L, Qi T, Zhang Y, Chu J. Morphosynthesis route to large-pore MCM41 microspheres, *Microporous and mesoporous materials*; 2006 Apr 15; 91(1-3):156-60. [[Crossref](#)], [[Google Scholar](#)], [[Publisher](#)]
39. Wang Y, Zhang F, Wang Y, Ren J, Li C, Liu X, Guo Y, Guo Y, Lu G. Synthesis of length controllable mesoporous MCM41 rods, *Materials Chemistry and Physics*; 2009 Jun 15; 115(2-

- 3):649-55. [[Crossref](#)], [[Google Scholar](#)], [[Publisher](#)]
40. Kokunešoski M, Gulicovski J, Matović B, Logar M, Milonjić SK, Babić B. Synthesis and surface characterization of ordered mesoporous silica MCM41, *Materials Chemistry and Physics*; 2010 Dec 1; 124(2-3):1248-52. [[Crossref](#)], [[Google Scholar](#)], [[Publisher](#)]
41. Anunziata OA, Beltramone AR, Martínez ML, Belon LL. Synthesis and characterization of SBA-3, MCM41, and SBA-1 nanostructured catalytic materials, *Journal of colloid and interface science*; 2007 Nov 1; 315(1):184-90. [[Crossref](#)], [[Google Scholar](#)], [[Publisher](#)]

HOW TO CITE THIS ARTICLE

Parastoo Seyedmohammadi, Neda Kouhzadi, Alireza Taheri. Intensification of Catalytic Oxidative Desulfurization by MCM41 Supported Ionic Liquid-Cd-HPMo Composite Activating H₂O₂ System and Mechanism Insight. Prog. Chem. Biochem. Res., 6(4) (2023) 327-340

 <https://doi.org/10.48309/10.48309/pcbr.2023.411107.1278>

 https://www.pcbiochemres.com/article_182709.html

